Chemistry–A European Journal
Research Article
doi.org/10.1002/chem.202303673
Chemistry Europe
European Chemical Societies Publishing
www.chemeurj.org

Self-Assembled Supported Ionic Liquids

Cindy-Ly Tavera-Méndez[+],[a] Alexander Bergen[+],[b] Simon Trzeciak,[c] Frank W. Heinemann,[b] Robert Graf,[d] Dirk Zahn,[c] Karsten Meyer,*[b] Martin Hartmann,*[a] and Dorothea Wisser*[a]

Separation and reuse of the catalytically active metal complexes are persistent issues in homogeneous catalysis. Supported Ionic Liquid Phase (SILP) catalysts, where the catalytic center is dissolved in a thin film of a stable ionic liquid, deposited on a solid support, present a promising alternative. However, the dissolution of the metal center in the film leaves little control over its position and its activity. We present here four novel, task-specific ionic liquids [FPh_nIm^HR]I (n = 1, 2; R = PEG_2, $C_{12}H_{25}$), designed to self-assemble on a silica surface without any covalent bonding and offering a metal binding site in a controlled distance to the support. Advanced multinuclear solid-state NMR spectroscopic techniques under Magic Angle Spinning, complemented by molecular dynamics (MD) simulations, allow us to determine their molecular conformation when deposited inside SBA-15 as a model silica support. We provide here conceptual proof for a rational design of ionic liquids self-assembling into thin films, opening an avenue for a second, improved generation of SILP catalysts.

Introduction

Supported Ionic Liquid Phase catalysts (SILPs) have emerged in the past two decades as a promising alternative to classic homogeneous or heterogeneous catalytic systems. In SILPs, a thin film of an ionic liquid (IL) is dispersed over the surface area of a porous solid. The catalytically active metal complex is dissolved in the IL film. Macroscopically, SILPs are solids, while the catalytic reaction takes place in a liquid environment. SILP materials, therefore, combine the uniformity of catalytic sites and the high control over the selectivity with the ease of processing of heterogeneous catalysts. As a consequence, SILP materials have already found their way to industrial applications.[1–3]

In SILP catalysts, the position of the metal center in the film, its solubility, and the diffusion limitation of reactants in the IL phase will influence reactivity and selectivity. Orientation and confinement effects may play a role if molecular catalysts assemble at the solid/liquid interface. Depending on the interface activity of the ligand, the choice of the IL, and the support material, the catalyst has been found to be significantly enriched at the solid/liquid or the liquid/gas interface.[4,5]

Therefore, to fully exploit the potential of SILP catalysts, controlling the position of the catalyst inside the IL film may strongly improve the control over the catalytic reaction. Covalent binding of the catalyst to the surface has been proposed,[6] however, covalent bonds may be cleaved under reaction conditions. Here, we follow a different approach, which relies on self-assembly based on non-covalent interactions, allowing for a dynamic and potentially reversible orientation of the IL molecules and the catalyst relative to the surface of the porous support. We present a set of four novel ionic liquids, which are tailored to act both as IL for film formation and as *N*-heterocyclic carbene (NHC) precursors for a potential noble metal catalyst (Scheme 1). These task-specific ionic liquids (**1**–**4**) are composed of a terminal fluorine group as "anchor" group for non-covalent binding to a silica support, a phenylene-based spacer (Ph_n, with n = 1 or 2) to vary the distance of the active site to the support, an imidazolium-based cation (Im^H) as NHC-precursor with iodide as counter anion, and either a polar polyethylene glycol-based side chain (R = PEG_2) or a non-polar dodecyl chain (R = $C_{12}H_{25}$), respectively. The latter are likely to orient toward the liquid/gas interface and ensure solubility for both polar and non-polar reactants. PEG_2-chains further enable proton transport to the catalytic site by hydrogen-bonding interactions.

From **1**–**4**, four pre-catalytic SILP materials (**SILP-1**–**SILP-4**) were prepared by deposition on SBA-15 as a model silica support with a well-defined structure and a narrow mesopore size distribution.[7] The interaction of the fluorine with the silica

[a] C.-L. Tavera-Méndez,[+] Prof. Dr. M. Hartmann, Dr. D. Wisser
Erlangen Center for Interface Research and Catalysis (ECRC)
Friedrich-Alexander-Universität Erlangen-Nürnberg (FAU)
Egerlandstraße 3, 91058 Erlangen (Germany)
E-mail: martin.hartmann@fau.de
dorothea.wisser@fau.de

[b] A. Bergen,[+] Dr. F. W. Heinemann, Prof. Dr. K. Meyer
Chair of Inorganic and General Chemistry
Department of Chemistry and Pharmacy
Friedrich-Alexander-Universität Erlangen-Nürnberg (FAU)
Egerlandstraße 1, 91058 Erlangen (Germany)
E-mail: karsten.meyer@fau.de

[c] S. Trzeciak, Prof. Dr. D. Zahn
Computer Chemistry Center (CCC)
Department of Chemistry and Pharmacy
Friedrich-Alexander-Universität Erlangen-Nürnberg (FAU)
Nägelsbachstraße 25, 91052 Erlangen (Germany)

[d] Dr. R. Graf
Max Planck Institute for Polymer Research
Ackermannweg 10, 55128 Mainz (Germany)

[+] These authors contributed equally to this work.

Supporting information for this article is available on the WWW under https://doi.org/10.1002/chem.202303673

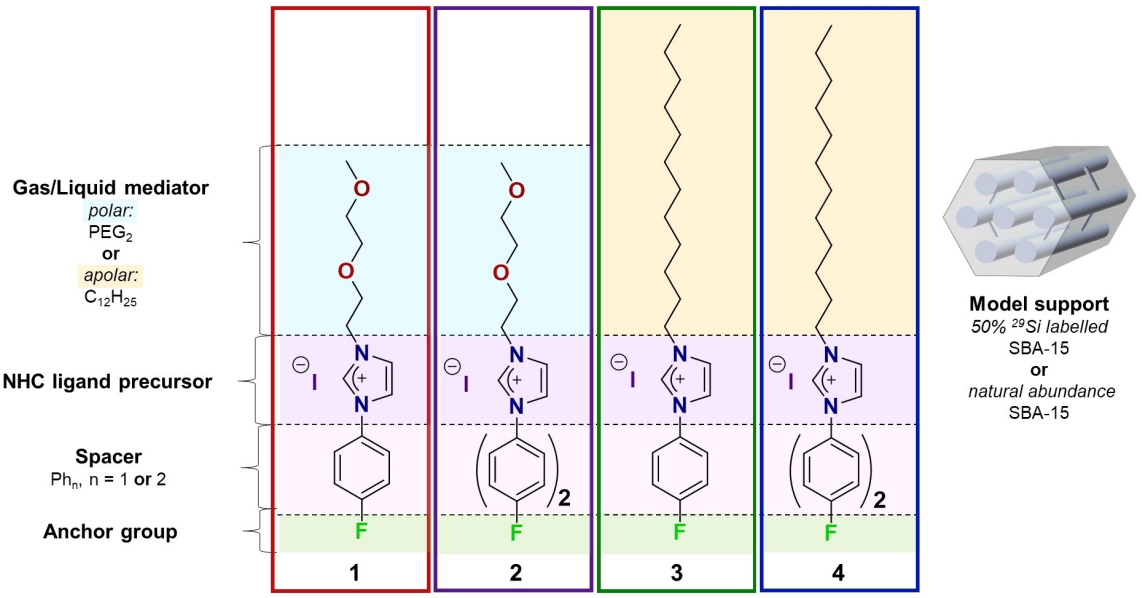

Scheme 1. Structure of fluorinated, task-specific ionic liquids (**1**–**4**) synthesized and used in this study (left). Structure model of the mesoporous silica material SBA-15, which was used as support to prepare the respective SILPs (right).

support, the orientation of the ILs towards the support, their conformation in the film, and the changes in the film with increasing loading were investigated in detail by a series of advanced multi-dimensional solid-state Magic Angle Spinning (MAS) NMR techniques. We find that in three of the SILPs, this fluorine self-assembles at a close distance to the silica surface for most of the molecular conformations.

Results and Discussion

Synthesis of Task-Specific Ionic Liquids

[FPhIm^{H}PEG$_2$]I (**1**) and [FPhIm^{H}C$_{12}$]I (**3**) could be synthesized directly by alkylation of the respective 1-(4-fluorophenyl) imidazole. The [1,1′-biphenyl] moiety was first prepared by a palladium-catalyzed Suzuki-Miyaura C–C cross-coupling of 1-(4-bromophenyl)imidazole and 4-fluorophenylboronic acid. The resulting 1-(4′-fluoro-[1,1′-biphenyl]-4-yl)imidazole was then alkylated similarly to the 1-(4-fluorophenyl)imidazole with 1-iodododecane or 1-iodo-2-(2-methoxyethoxy)ethane to form **2** and **4**, respectively (Scheme S1). ILs **1** and **3** were obtained as liquids, **2** (CCDC-2297930) and **4** (CCDC-2297931) as crystalline solids (Figure S1).

NMR Spectroscopy in Solution

All four ionic liquids (**1**–**4**) were characterized by ^{1}H, ^{13}C, and ^{19}F NMR spectroscopy in solution (Figure S5–S7), illustrating their purity and structural similarity. Details can be found in the Supporting Information.

In the ^{19}F NMR spectra of **1**–**4**, a single multiplet was observed for each compound (Figure S7). For **1** and **3**, the ^{19}F signal arises at -108.6 ± 0.1 ppm, the signals of **2** and **4** are high-field shifted toward -113.45 ± 0.05 ppm.

Solid-State Molecular Structures

Colorless, block-shaped single-crystals of **2** and colorless needles of **4** suitable for X-ray diffraction analysis (XRD) were obtained from an oversaturated solution of **2** in tetrahydrofuran and by diffusion of diethyl ether into a solution of **4** in acetonitrile, respectively. While the dodecyl substituent is packed linearly (Figure 1), the PEG$_2$ chain is orientated in a twisted way (Figure 2), which is common for long alkyl- and oligomeric alkoxy-substituents, respectively.[8–10]

The triclinic unit cell of **2** consists of two ion pairs in the centrosymmetric P$\bar{1}$ space group. Hence, when viewed in the direction of the crystallographic *a* axis (Figure S9), the ^{F}Ar–Ar–Im moieties of the two cations are placed on top of each other, pointing in opposite directions. In this way, the ^{F}Ar–Ar–Im moieties form a layered structure along the crystallographic *a* axis with the middle phenylene rings orientated in a parallel but alternately shifted fashion (Figure S10). The PEG$_2$ substituents from different unit cells interact with the cationic imidazolium rings as well as the iodide anions. Thus, the PEG$_2$ chains interlink adjacent unit cells mainly in the directions of the crystallographic *a* and *c* axes (Figure S11). This possibly accounts for the non-linear packing of the PEG$_2$ substituents in the crystals of **2**. Additionally, repulsive interactions of the oxygen electron lone pairs on different ether groups[10] are also avoided by the twisting of the PEG$_2$ chains.

The orthorhombic unit cell of **4**, on the other hand, comprises eight ion pairs in the centrosymmetric *Pbca* space group. The non-polar C$_{12}$ chains are separated from the polar regions in crystals of ionic compounds.[8] Thus, the ^{F}Ar–Ar–Im

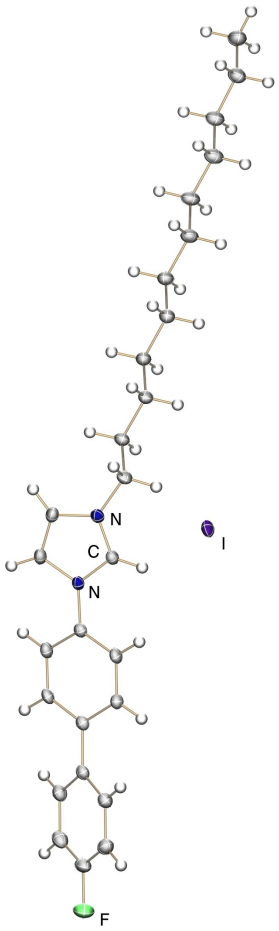

Figure 1. Solid-state molecular structure of [$FPh_2Im^HPEG_2$]I (**2**). Thermal ellipsoids are shown at 50% probability. Color code: C – grey, H – white, N – blue, O – red, F – green, I – violet.

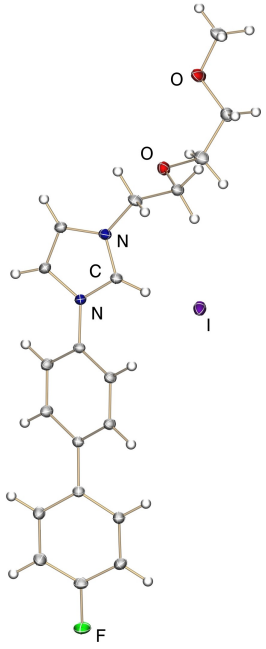

Figure 2. Solid-state molecular structure of [$FPh_2Im^HC_{12}$]I (**4**). Thermal ellipsoids are shown at 50% probability. Color code: C – grey, H – white, N – blue, F – green, I – violet.

moieties of **4** are not forming parallel, layered structures, but the crystals are comprised of regions in which ionic/polar interactions (imidazolium cations and iodide anions) and dispersive interactions (C_{12} and ^{F}Ar–Ar substituents), respectively, predominate (Figure S13). This tendency necessitates the four stacked pairs of ^{F}Ar–Ar–Im moieties in each unit cell to be alternately rotated, resulting in a herringbone packing arrangement (Figure S14), possibly to minimize repulsive (cat)ionic interactions.

Characterization of Support Materials

SBA-15 was chosen as a well-defined amorphous silica model support material.[7] To gain sensitivity in multinuclear 2D MAS NMR experiments, SBA-15 was prepared with approx. 50% of a fully ^{29}Si-labelled precursor. Added to the ^{29}Si natural abundance of 4.7%, this leads to an overall ^{29}Si percentage of 52.1%. Small-angle X-ray scattering (SAXS) diffractograms (Figure S15) of the ^{29}Si-enriched material and the SBA-15 with ^{29}Si at natural abundance exhibit peaks at (100), (110), (200), (210), and (300), indication of a high structural ordering, characteristic of a 2D hexagonal lattice (*p6mm*) displayed typically by SBA-15 silica.[11,12] The d_{100} spacings were 8.7 nm and 8.9 nm, respectively.

The nitrogen physisorption isotherms correspond to type IV isotherms with an H1 hysteresis loop, typical for ordered mesoporous silicas like SBA-15 (Figure S16a–b).[13] A narrow and uniform pore size distribution centered at around 6 nm is evidenced in both supports (Figure S16c–d). Scanning electron microscope (SEM) images (Figure S17) display the distinctive morphology for SBA-15 materials, agglomerated rod-like particles, in both cases.

SILP Preparation

To understand the interaction of the IL and the support, without possible influences from the catalyst, we did not include the latter in this study. Consequently, the term SILP materials instead of SILP catalysts is used. A low pore-filling degree α_{IL} of about 10% was chosen to avoid the formation of a bulk phase.

The obtained labeled SILP materials (Table 1 and Table S5) are white to yellowish powders with the morphology of the SBA-15 parent material (Figure S18).

Table 1. Overview of the prepared, labeled SILP materials.

Sample	Ionic Liquid	Support	Calc. Pore-Filling Degree (α_{IL})
SILP-1	[$FPhIm^HPEG_2$]I (**1**)	50% ^{29}Si-enriched SBA-15	11%
SILP-2	[$FPh_2Im^HPEG_2$]I (**2**)		10%
SILP-3	[$FPhIm^HC_{12}$]I (**3**)		11%
SILP-4	[$FPh_2Im^HC_{12}$]I (**4**)		12%

SILP materials were prepared with a ^{29}Si natural abundance SBA-15 (Table S6) for experiments where ^{29}Si sensitivity enhancement was irrelevant. ^{19}F 1D NMR spectra confirm that the fluorine environments, and in consequence, the F–Si interaction, are maintained independently from the ^{29}Si content (compare Figure 3 and Figure 4).

^{19}F MAS NMR: Ionic Liquid Behavior upon Deposition

The ^{19}F MAS NMR spectra of the pure liquid ILs (**1** and **3**) exhibit a single narrow resonance at nearly identical chemical shifts of −110.8 ppm and −110.0 ppm, respectively (Figure 3a and c, bottom). In the case of ILs that are solid at room temperature (**2** and **4**), broader single resonances at −114.1 ppm and −114.6 ppm, respectively, are observed (Figure 3b and d, bottom). The different ^{19}F chemical shifts between liquid and solid ILs may be explained by the chemical environment including through-space interactions to neighboring molecules, which will necessarily differ between liquid and solid state.

Upon impregnation, fitting of the ^{19}F MAS NMR spectra revealed the presence of two overlapped resonances (Figure 3, top spectra). In three SILP materials, one of the signals appears shifted downfield (δ_1(^{19}F)), and the second (δ_2(^{19}F)) shifted upfield compared to the resonance of the pure compound; only in **SILP-2**, the pure IL signal is superimposed with the downfield signal δ_1(^{19}F) (Figure 3b). From these spectra, a cleavage of the C–F bond and a covalent binding of fluorine to the silica surface can be excluded since, in that case, ^{19}F chemical shifts in Si–F bonding would be expected at much lower values (−130 ppm to −150 ppm).[14,15] Instead, we suggest that new resonances arise from the interactions of the fluorine moiety and the support. The presence of two distinct peaks points toward distinct interaction sites with different local chemical environments. The resonances of the deposited ionic liquids are broader than the parent bulk IL, supporting the hypothesis of an adsorbed state on the support (Table S8).

Additionally, we performed a preliminary test on materials **SILP-1** and **SILP-4** to assess the temperature stability of both fluorine environments. The samples were exposed to 493 K for 3 h and subsequently cooled down naturally or quenched with liquid nitrogen. The ^{19}F MAS NMR spectra (Figure S19) of the treated samples show that both fluorine resonances remained unchanged, suggesting stability of the SILP materials at high temperatures, with the potential to recover their initial state after the treatment.

The two fluorine chemical shifts were systematically observed with pore-filling degrees α_{IL} ranging from 5 to 55% (Figure 4a–b). The signal intensity increases with loading. However, for the high IL loadings ($\alpha_{IL} > 20$%), the deconvolution clearly shows a third resonance (δ_3(^{19}F)) at the chemical shift of the pure, bulk ionic liquid (Figure S20). This resonance also exhibits a smaller FWHM than that of resonances δ_1(^{19}F) and δ_2(^{19}F). The chemical shift value and signal narrowing suggest

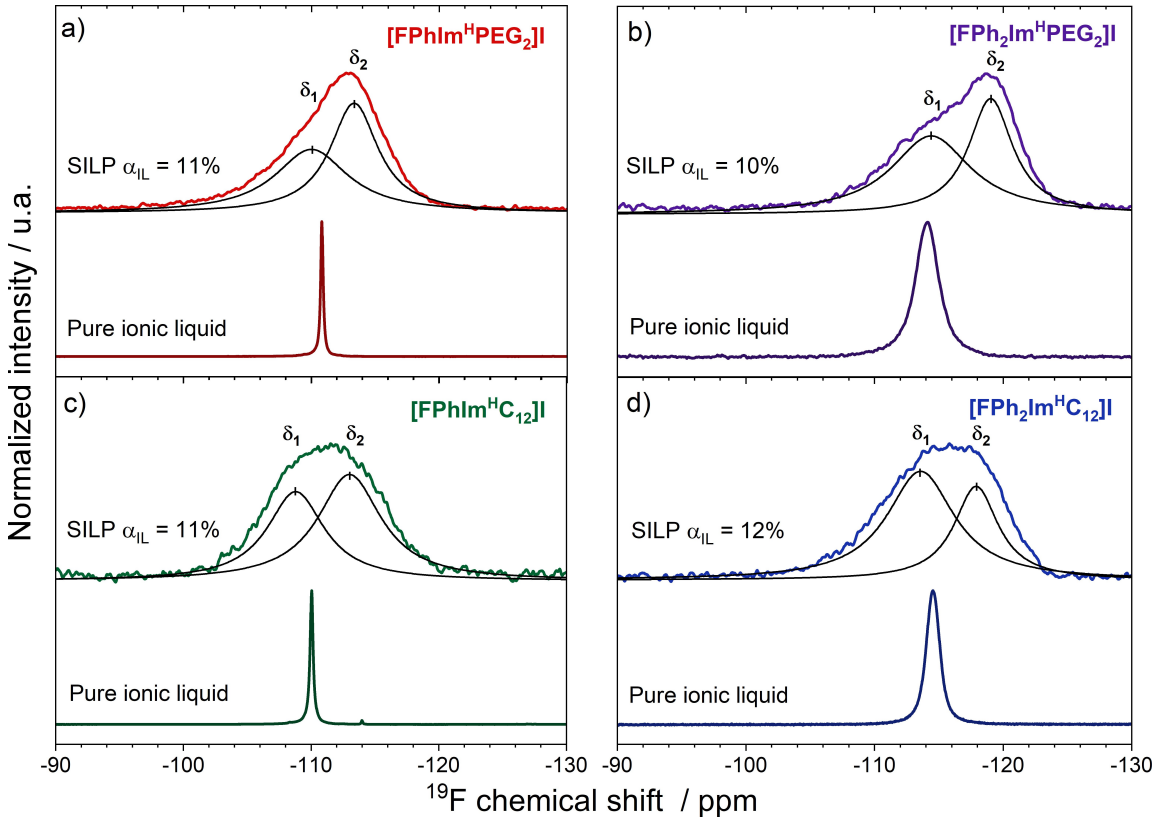

Figure 3. ^{19}F MAS NMR spectra of (a) **1**, (b) **2**, (c) **3**, and (d) **4**. While the spectra of pure ionic liquids (lower spectra) were acquired under static conditions, 25 kHz MAS was applied for the respective SILP materials (**SILP-1** to **SILP-4**), supported on 50% ^{29}Si-enriched SBA-15 with a pore-filling degree (α_{IL}) of 10 or 11% (upper spectra).

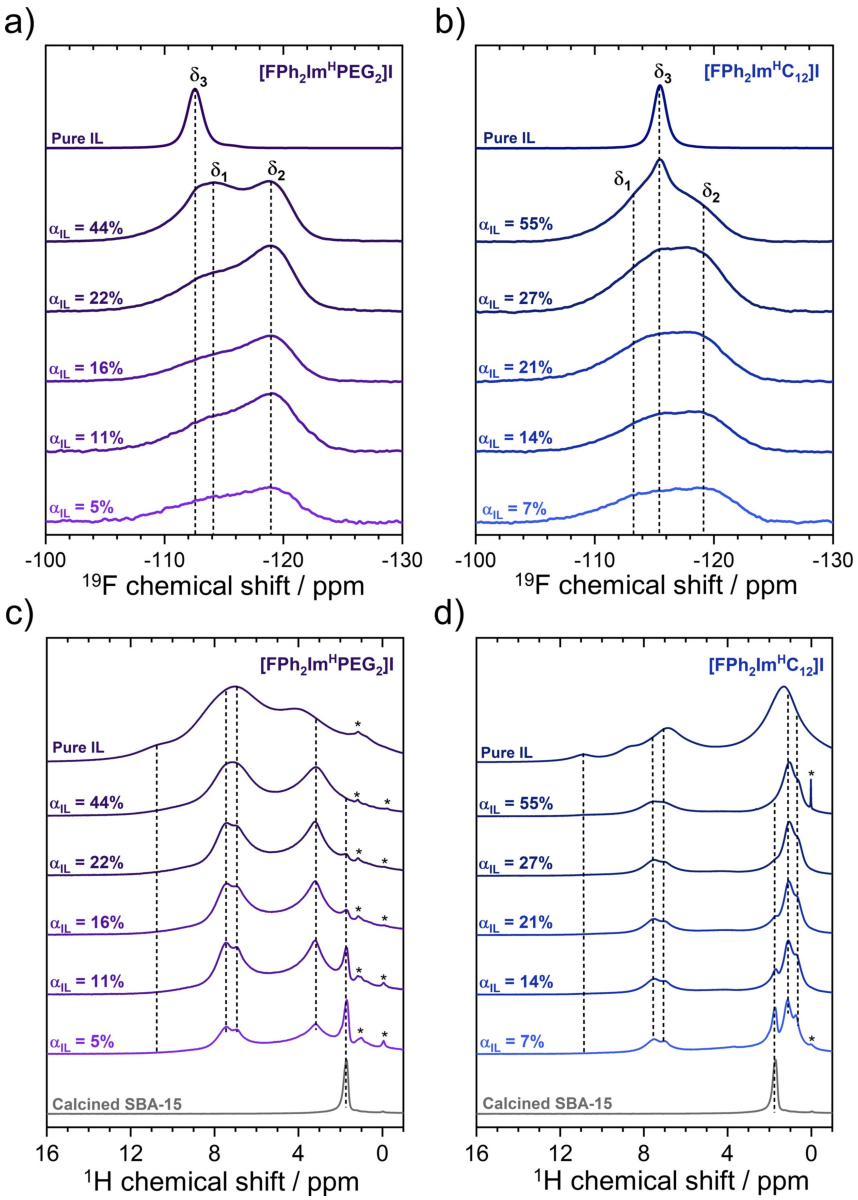

Figure 4. ^{19}F (top) and ^{1}H (bottom) MAS NMR spectra at 30 kHz MAS of (a, c) **SILP-2** and (b, d) **SILP-4**, supported on natural abundance SBA-15 with varying pore-filling degree (α_{IL}). The spectra for the pure ILs (**2** and **4**) and calcined natural abundance SBA-15 are added for comparison. Resonances from impurities are marked with asterisks (*).

the presence of a third chemical environment, $\delta_3(^{19}F)$, corresponding to a fluorine population without a F–Si interaction with the surface.

The ^{1}H MAS NMR spectrum of the SBA-15 support prior to IL impregnation (Figure 4c and d, grey line) exhibits a single resonance at 1.7 ppm attributed to isolated silanol groups on the silica surface.[16–18] The ^{1}H MAS NMR spectra of deposited ILs exhibit a combination of the resonances from the IL and the support (Figure 4c and d, Figure S21). In the MAS NMR spectra of the SILPs, protons of the different substituents (phenyl, biphenyl, PEG_2, and C_{12}) or the imidazolium ring could be assigned (Figure S23). When the IL loading is increased, the characteristic bulk-like behavior of the IL resonances is evidenced by broader and merging resonances, while the silanol resonance from the support decreases in intensity (Figure 4c and d). We have recently found a correlation between decreased silanol resonance intensity and hydrogen bond (HB) formation within a series of commercial imidazolium-based ILs deposited on silica-60, MCM-41, and SBA-15.[19] In those systems, a complete disappearance of the silanol resonance indicates a complete surface coverage, as was found before by Haumann et al.[20] However, as the binding behavior in the set of ILs presented here may be different, the latter correlation may not be applicable.

The pore-filling of the **SILP-2** and **SILP-4** materials was further studied by nitrogen physisorption. Their isotherms show similar behaviors to the parent SBA-15 support and were classified as type IV isotherm featuring an H1 hysteresis loop

(Figure S24).[13] The hysteresis shape is maintained along the full studied range, evidence of uniform cylindrical pores without pore blocking, even at high pore-filling degrees.[21] With increasing IL loading, the average pore widths decrease (Figure S25a and b), and a progressive reduction of the total pore volume (Figure S25c) is observed. The pore width difference in each IL increase is smaller than the length of one IL molecule (~18–20 Å). However, we note that nitrogen physisorption brings with it several sources of uncertainty: nitrogen may be soluble in the IL, and the nitrogen molecule may specifically interact with different functional groups, leading to varying orientations on different surfaces.[22] Therefore, we carefully suggest an incomplete surface coverage at the low pore-filling degrees, followed by successive addition of IL molecules to a monolayer on the surface. This finding is in line with the ^{19}F MAS NMR spectra (Figure 4b and d), in which the appearance of $\delta_3(^{19}F)$ at the chemical shift of the pure IL indicates the formation of a bulk IL phase inside the pores.

^{19}F→^{29}Si Cross Polarization (CP MAS): Nuclear Proximity

To further probe fluorine–support interactions, ^{29}Si direct excitation (DE) MAS NMR spectra of the enriched SBA-15 and ^{19}F→^{29}Si cross-polarization (CP MAS) spectra of the SILP materials were acquired (Figure 5). ^{29}Si DE MAS NMR spectra of silicon dioxide (SiO_2) materials present the well-known resonances of "Q^n sites" at −90.3 ppm (Q^2), at −98.3 ppm (Q^3), and at −106.7 ppm, (Q^4).

Magnetization transfer by CP between ^{19}F and ^{29}Si will efficiently occur only if the two spins are in close proximity, and the mobility of the spins is low.[23] For the SILP materials, the presence of ^{29}Si CP signals confirms a close interaction of the fluorine moiety with the support and, thus, a short F–SBA-15 distance, within a distance of a few Å. Interestingly, we do observe ^{29}Si CP signals similar to those displayed by the solid ILs (**2** and **4**) also for the SILPs containing the liquid ILs (**1** and **3**), suggesting that the liquid ILs are somewhat immobilized on the support. Compared to ^{1}H–^{29}Si CP MAS spectra (Figure S26), recorded with the same contact time of 4 ms, the Q^3 to Q^4 resonance ratio is lower in the ^{19}F–^{29}Si CP MAS spectra. This suggests a preferred interaction of the fluorine sites to the Q^4 groups on the surface. A less intense resonance, around −101 ppm, accounts for a second F–Si interaction with the Q^3 sites. A higher pore-filling degree, **SILP-4** at 40 % α_{IL} (Figure S27), exhibits similar results, the Q^4 resonance being even more predominant than at lower pore-filling degrees.

Note that due to the low signal intensity of the ^{19}F→^{29}Si CP spectra, we did not attempt to record ^{19}F–^{29}Si HETCOR spectra.

Similar interactions of fluorine groups with silica were demonstrated before by MAS NMR on the complex [Pd(dppp)(dtc)]BF_4, supported on silica but not covalently bound,[24] and for (pentafluorophenyl)propyl groups in short polymers covalently bound to silica nanoparticles.[25]

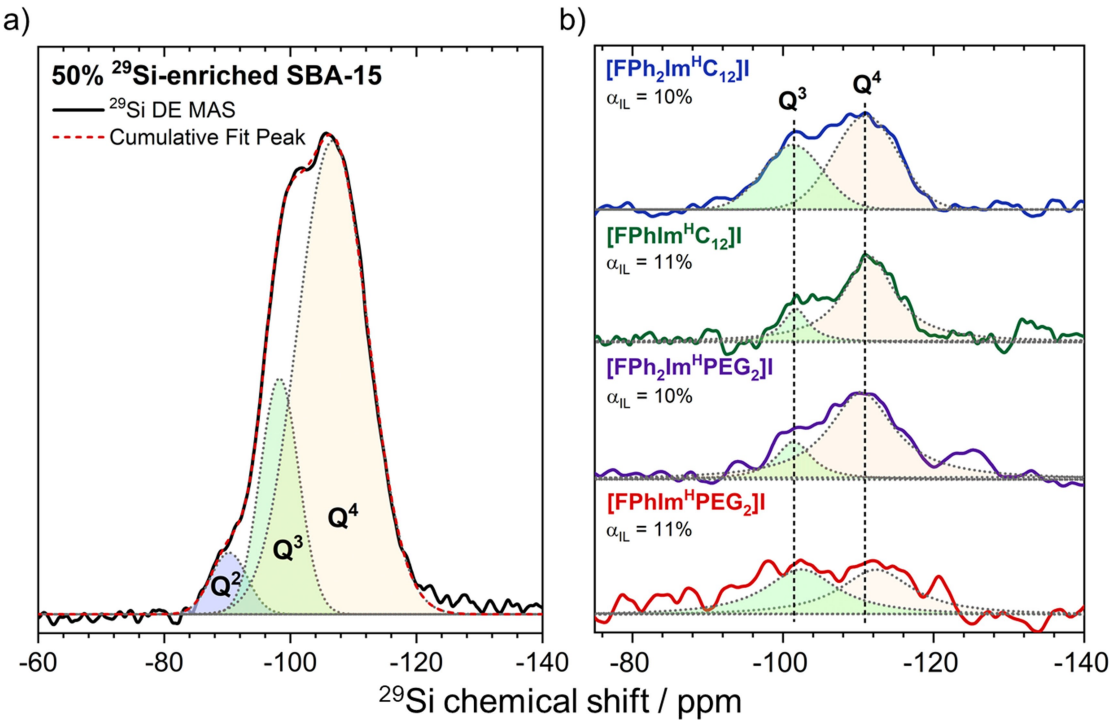

Figure 5. (a) ^{29}Si MAS NMR spectrum at 25 kHz of calcined ^{29}Si-enriched SBA-15, obtained by DE and (b) ^{19}F→^{29}Si CP MAS NMR spectra of SILP materials, supported on 50 % ^{29}Si-enriched SBA-15 with a pore-filling degree (α_{IL}) of 10 or 11 %. **SILP-1** (red), **SILP-2** (purple), **SILP-3** (green), and **SILP-4** (blue).

Distance of the ^{19}F–^{29}Si Spin Pair from Rotational Echo Double Resonance (REDOR)

The F–Si internuclear distances for the SILP materials were estimated with $^{19}F\{^{29}Si\}$ rotational-echo double resonance (REDOR) NMR spectroscopy. The REDOR experiment allows for the measurement of the heteronuclear dipolar coupling constant, D_{F-Si}, of, ideally, an isolated interacting spin pair under MAS conditions. The dipolar coupling constant contains distance information through a $1/r^3$ dependence.[26,27] The full signal ^{19}F spectra (S_0) and the attenuated signal (S) spectra were deconvoluted into the two resonances, $\delta_1(^{19}F)$ and $\delta_2(^{19}F)$. The REDOR signal fraction S/S_0 was plotted as a function of the recoupling time (Figure 6 and Table S9), using a Matlab® script adapted from Berruyer et al.[28]

In the **SILP-2** and **SILP-4** materials from solid ILs, both fluorine environments $\delta_1(^{19}F)$ and $\delta_2(^{19}F)$ show REDOR dephasing (Figure 6b and c); thus, their fluorine atoms are close to silicon nuclei within a distance (r_{F-Si}) of 2.4 to 3.1 Å (Table S9). Overall, the resonance $\delta_1(^{19}F)$ has a larger dipolar coupling, related to a short distance between the spin pairs (2.36 and 2.54 Å, respectively). The more shielded environment, $\delta_2(^{19}F)$, presents slightly longer internuclear distances of 3.12 and 2.58 Å, respectively. We note here that these ^{19}F–^{29}Si distances are shorter than the sum of the van-der-Waals radii of the atoms (3.6 Å for F–Si), short enough to indicate non-covalent electrostatic interactions between F and Si.

For the $\delta_1(^{19}F)$ resonance, the dephasing plateau is located at $S/S_0 \approx 0$.

In contrast, the resonance at $\delta_2(^{19}F)$ of **SILP-2** and **SILP-4** does not dephase to 0, but levels off at a REDOR fraction of ~0.4. Several scenarios might explain this finding: Dephasing plateaus of non-zero values ($S/S_0 > 0$) have been found if partial mobility of the interacting spin pair averages some dipolar couplings to zero,[29–31] or if a fraction of the observed spins (^{19}F) are far away from any dephased spin (^{29}Si),[28,32] and experience only negligible dipolar coupling. On the surface of 50% ^{29}Si-enriched silica, also three-spin systems ($^{29}Si_a$–^{19}F–$^{29}Si_b$) may occur, for which non-zero dephasing plateaus have been observed in specific geometries.[31,33] As the precise geometry of the fluorine groups on the surface in unknown, a two-spin approximation is used here. With this model, the presence of three-spin systems might lead to a slight overestimation of the dipolar couplings and a slight underestimation of the ^{19}F–^{29}Si distances.[31,33] Importantly, however, MD simulations show that the fluorine group points away from the silica surface for a part of the molecules (see below), thus supporting the 2nd scenario.

For comparison, we also recorded REDOR spectra on a **SILP-4** material with a high pore filing degree of 40%. Again, the resonance $\delta_1(^{19}F)$ at −113 ppm dephases with a short F–Si distance of 2.07 Å (Figure S29 and Table S10). The strong overlap of the resonances $\delta_2(^{19}F)$ and $\delta_3(^{19}F)$ leads to large uncertainties of the deconvoluted signal areas. Overall, no clear dephasing behavior is observed for these two resonances. At this high degree of pore-filling, indeed only a smaller part of the fluorinated groups may be close to the silica support.

In the **SILP-1** material prepared from a liquid IL, only the resonance $\delta_1(^{19}F)$ at −110 ppm dephases, yielding a short F–Si distance of 2.05 Å with a dephasing plateau at $S/S_0 \approx 0.4$ (Figure 6a). The absence of dephasing of the $\delta_2(^{19}F)$ resonance of **SILP-1** indicates either very mobile or no interacting spin pairs. The more dynamic behavior of **SILP-1** is confirmed by ^{19}F exchange spectra (EXSy, Figure S28), showing a cross peak between the $\delta_1(^{19}F) \leftrightarrow \delta_2(^{19}F)$ sites, at a shorter mixing time for **SILP-1** (5 ms; Figure S30) than for **SILP-2** (80 ms; Figure S29b). These cross signals are evidence of chemical exchange, i.e., "hopping" between the two different sites. Therefore, although the IL molecules are self-assembled on the surface, the dynamic exchange of these molecules between different sites may average some dipolar couplings with ^{29}Si to zero. For **SILP-3**, no REDOR dephasing was observed.

In summary, the REDOR data unambiguously show that in the **SILP-2** and **SILP-4** materials, a majority of the fluorine atoms are in very close proximity to the silica surface. Such a stable ^{19}F–^{29}Si interaction is even visible in **SILP-1** which contains a liquid IL.

IL Arrangement on Silica Surface from 2D MAS NMR Spectra

Heteronuclear correlation (HETCOR) experiments between ^1H–^{29}Si and ^1H–^{19}F, and proton double quantum coherence experiments (^1H SQ-DQ), were recorded to shed light onto the IL conformation inside the SBA-15 pores.

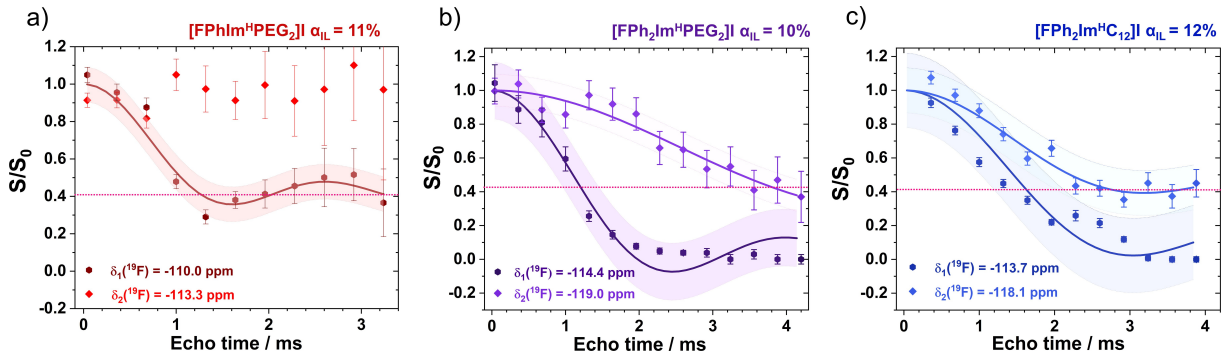

Figure 6. Experimental (symbols) and best numerical fitting (solid lines) $^{19}F\{^{29}Si\}$ REDOR dephasing curves at 25 kHz MAS of (a) **SILP-1**, (b) **SILP-2**, and (c) **SILP-4**, supported on 50% ^{29}Si-enriched SBA-15 and obtained after deconvolution of the two overlapping resonances, $\delta_1(^{19}F)$ (squares) and $\delta_2(^{19}F)$ (diamonds). Error bars display the standard deviation on S/S_0 calculated by error propagation.

^{1}H–^{29}Si HETCOR spectra (Figure 7) were obtained at short (3 ms) and long (8 ms) contact times (t_c). The spectra at short t_c preferentially display the correlation of nuclei interacting at a short distance range. Acquisition under longer t_c displays the interaction with proximal and distant nuclei. The spectra show the resonances of isolated silanols at 1.7 ppm, correlating with Q^2 and Q^3 sites. A resonance around 2.9 ppm is tentatively attributed to Q^3 silanol groups in an HB interaction with fluorine; this assignment is corroborated by ^{1}H–^{19}F HETCOR spectra (see below). At short t_c (Figure 7a and c), an interaction of either PEG_2 protons between 3–5 ppm for **SILP-2** or the dodecyl protons between 0–1 ppm in **SILP-4** with the Q^3 sites is visible. Only after a t_c of 8 ms (Figure 7b and d), weaker correlations with the phenyl protons and imidazolium protons of the IL molecules are observed. The appearance order of cross-correlations with increasing contact times suggests that IL molecules are not deposited in a flat conformation on the surface, but in an upright position. However, the correlations at short t_c of PEG_2 or C_{12} chains with the silica indicate that these groups are close to the surface, at least in some of the molecules. It is possible that either the ILs are arranged in the opposite direction – fluorine atoms pointing away from the surface – or that some flexible alkyl or PEG_2 chains fold over, bringing them closer to the silica surface.

^{1}H–^{19}F HETCOR at varying contact times of the four impregnated ILs over ^{29}Si-labelled SBA-15 at a pore-filling degree of ~10 % were carried out to obtain information on the arrangement of fluorine on the silica surface (Figure 8 and Figure S31). The HETCOR spectra of liquid IL-based SILPs showed weaker intensities but similar signals (Figure S31a and c). As expected, the short contact time spectra (t_c = 0.1 ms) present strong correlations between $\delta_1(^{19}F)$ and $\delta_2(^{19}F)$ and the neighboring aromatic protons (purple) at around ~7 ppm. Cross-correlations in the region between 0 and 4 ppm in the proton dimension and $\delta_2(^{19}F)$ appeared, which result from the interaction of the PEG_2 or alkyl chain, as well as from what appears to be the interaction of silanol groups with $\delta_2(^{19}F)$. Since HB formation is known to induce deshielding effects, it is

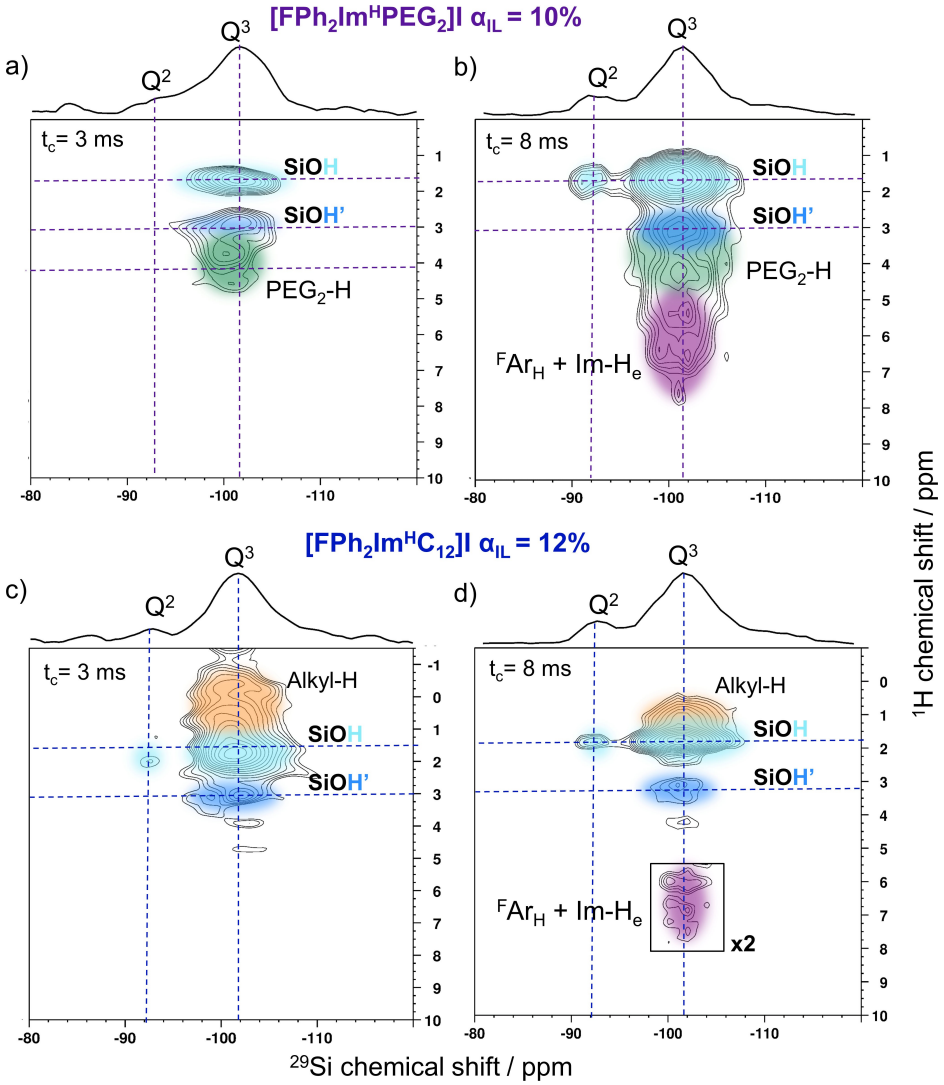

Figure 7. ^{1}H–^{29}Si HETCOR NMR spectra at 30 kHz MAS of (a, b) **SILP-2** and (c, d) **SILP-4**, supported on 50 % ^{29}Si-enriched SBA-15 with a pore-filling degree (α_{IL}) of 10 %. The spectra were acquired at varying contact times (t_c) of 3 and 8 ms.

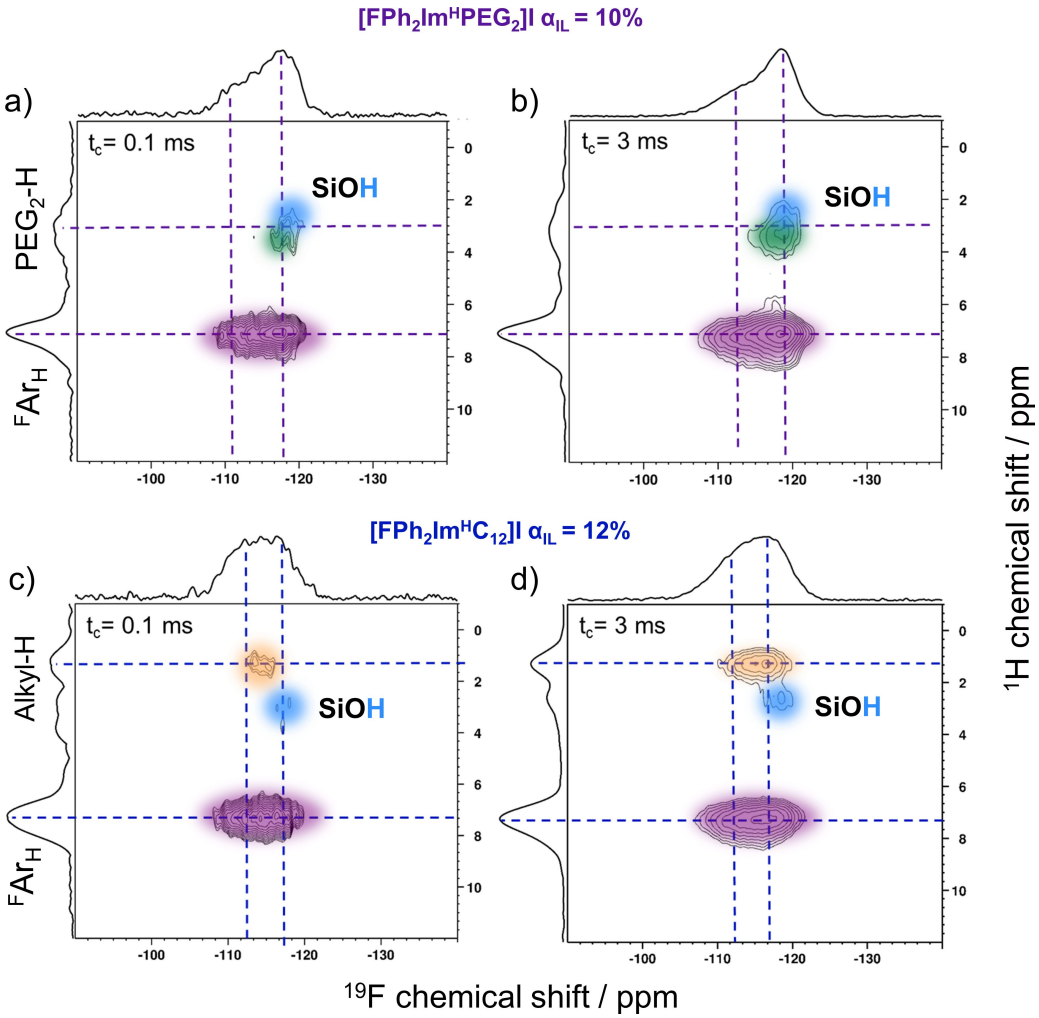

Figure 8. ^{1}H–^{19}F HETCOR NMR spectra at 30 kHz MAS of (a, b) **SILP-2** and (c, d) **SILP-4**, supported on 50% ^{29}Si-enriched SBA-15 with a pore-filling degree (α_{IL}) of 10%. The spectra were acquired at varying contact times (t_c) of 0.1 and 3 ms.

proposed that the silanol resonance at 1.7 ppm is engaged in an HB interaction with the population at $\delta_2(^{19}F)$ and, in consequence, moves to a higher chemical shift. This hypothesis is in agreement with the results of the 1D ^{19}F NMR spectra, which show $\delta_2(^{19}F)$ to be more shielded than the IL ^{19}F resonance of the bulk; the $^{19}F\rightarrow^{29}Si$ and $^{1}H\rightarrow^{29}Si$ CP, showing an interaction of fluorine with Q^3 sites, and the REDOR results, which evidence that the more shielded interacting species at $\delta_2(^{19}F)$ has a larger F–Si internuclear distance (Figure 6).

The ^{1}H–^{19}F HETCOR spectra also show that the ^{19}F atom at $\delta_2(^{19}F)$ is close to the PEG_2 chain in **SILP-2** (~3.4 ppm) or the C_{12} chain in **SILP-4** (~1.3 ppm). Especially at short contact times, this correlation should not appear if it originated from intramolecular contact only. This result could be attributed to an antiparallel orientation of the IL molecules, which is the molecular configuration in the single crystals (Figure S8, Figure S14), or, specifically for **SILP-4**, to a conformation where the C_{12} chain bends over towards the [1,1′-biphenyl] moiety.[8] This picture is corroborated by the presence of cross resonances PEG_2–aromatic or alkyl–aromatic in ^{1}H–^{1}H SQ-DQ experiments (Figure 9 and Figure S32). These correlations show up also in spectra at varying pore-filling degrees (Figure S32), suggesting the presence of this molecular configuration even at low IL loading.

Molecular Dynamics Simulations

To complement the solid-state NMR results, we performed molecular dynamics (MD) simulations of IL film deposition on silica (see Supporting Information for simulation details). A 2D-periodic amorphous silica slab model was adopted from Macht et al.[34] and subjected to depositing $[FPh_2Im^HC_{12}]I$ films, according to **SILP-4** (Figure 10a).

Since the exact monolayer density was not known, we initially placed an excess amount of 2000 IL pairs, leading to a film of several monolayers. After relaxation from simulated annealing, the resulting IL film at 300 K was analyzed by sampling occurrence profiles along the surface normal z. Figure 10a clearly indicates a layer-wise ordering of the IL, featuring three distinct layers of alternating FPh_2/alkyl, imidazolium-iodide, FPh_2/alkyl arrangements. While the occurrence

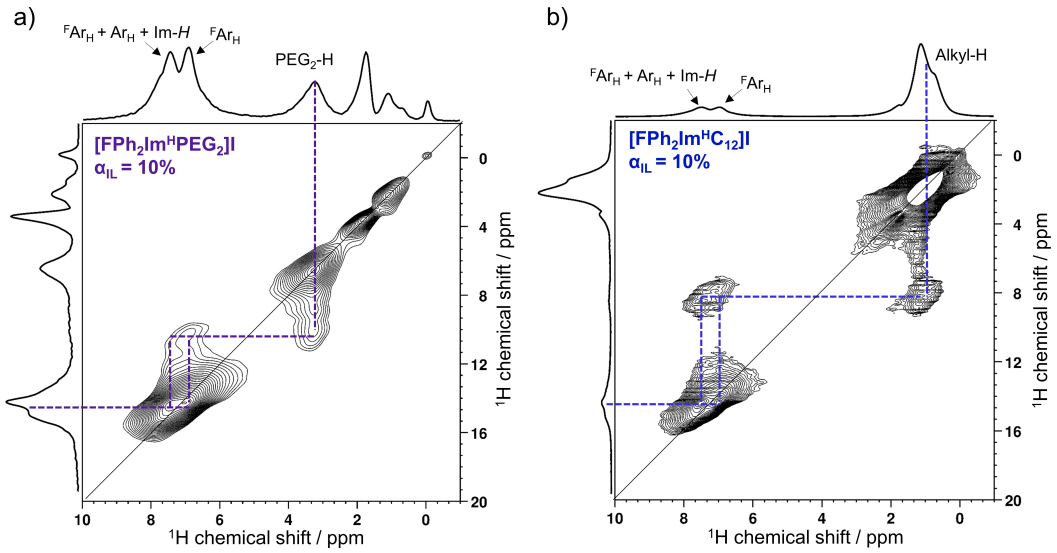

Figure 9. ^{1}H–^{1}H SQ-DQ at 30 kHz MAS of (a) **SILP-2** and (b) **SILP-4**, supported on 50% ^{29}Si-enriched SBA-15 with a pore-filling degree (α_{IL}) of 10%. The dashed lines indicate the cross correlation peaks.

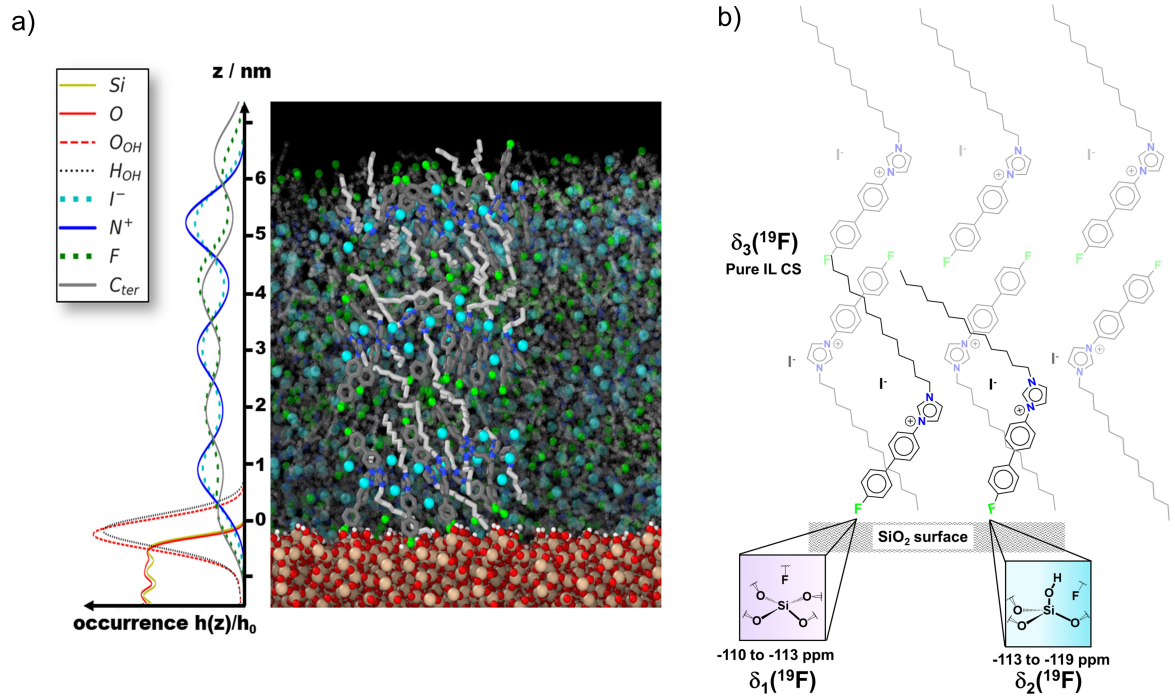

Figure 10. (a) MD simulation model of **SILP-4**: layer-wise ordering of (**4**). While the image shows three distinct layers, derived models of IL films featuring a single monolayer and a film of two full monolayers (3.1 resp. 3.1 + 2.9 ion pairs per nm^2) show analogous ordering (Figure S34). The MD simulations suggest a 40:60 of upward:downward orientation of FPh_2 moieties. (b) Schematic representation of the IL (**4**) supported on a silica surface.

profiles for Si, O, and OH indicate the roughness of the substrate model, the alignment of N and I densities is indicative of a two-dimensional packing triggered by Coulomb interactions. In turn, the terminal F and carbon (C_{ter}) atoms of the FPh_2 and the alkyl groups, respectively, show segregation from the polar domains. Based on the minima of the I^- occurrence profiles, the IL monolayer in contact with silica shows a thickness of about 2 nm and involves 3.1 IL pairs per nm^2. In turn, the next full monolayer is located from z = 1.8 to 3.9 nm and comprises a density of 2.9 nm^{-2} IL pairs. To confirm this, we performed two additional MD runs after cutting off excess IL pairs beyond the delimiters of one and two monolayer IL films, respectively. After relaxation, we find fully consistent occurrence profiles (Figure S34). Based on the monolayer IL film in contact to silica, we collected statistics for the alignment of the FPh_2 moieties. We find a 60:40 ratio of FPh_2 groups pointing towards vs. away from the silica surface.

Contacts to the silica surface are found as Si···F pairs and as OH···F interactions at a ~1.5:1 ratio. This is in good agreement with the intensity ratio of the resonances $\delta_1(^{19}F)$ and $\delta_2(^{19}F)$, which is 71:29 for **SILP-4** (Table S8). On average, less than half of the downward-oriented FPh_2 moieties show Si···F or OH···F bonding contacts according to the van-der-Waals criterion for hydrogen-bond like interactions of 3.6 and 2.6 Å, respectively. While this reflects a particularly strict selection demanding bonding, one may also use a more generous distance criterion such as 1.5 times the van-der-Waals distances. Indeed, within the latter thresholds we find that more than 80% of the downward-oriented FPh_2 moieties interact with silica.

In summary, we establish here a model for the arrangement of the fluorinated ILs on the silica surface that is coherent with all MAS NMR spectra recorded (Figure 10b). In all four SILP materials, IL molecules are present in at least two different conformations. In the solid-IL-based **SILP-2** and **SILP-4** materials, $^{19}F\{^{29}Si\}$ REDOR experiments indicate that both ^{19}F species are close to the silica surface in distances of approx. 2.5 to 3.1 Å (Figure 6b and c). Even in one of the liquid-IL-based SILPs (**SILP-1**), REDOR dephasing is evidence of the immobilization of one molecular conformation, with a short distance to the silica surface of approx. 2 Å (Figure 6a), despite the fact that the mobility of liquid molecules usually impedes any REDOR dephasing.

The MD simulations show that for a part of the molecules, the fluorinated end group is oriented away from the silica. Indeed, ^{19}F NMR spectra at higher filling degrees show a third fluorine population at $\delta_3(^{19}F)$ (Figure 4a and b). We attribute this chemical shift to IL molecules which are not in close contact with the silica surface.

We assume that the $\delta_2(^{19}F)$ resonance corresponds to ^{19}F nuclei in OH···F hydrogen bond with Q^3 silica sites, which is supported by the corresponding correlation in the ^1H–^{19}F HETCOR spectrum and the lower chemical shift (stronger shielding) of $\delta_2(^{19}F)$ (Figure 8). MD simulations confirm the presence of such hydrogen bonded OH···F pairs. ^{19}F–^{29}Si pairs in this contact exhibit a slightly longer internuclear distance. Only 60% of these fluorine spins are involved in an OH···F interaction, which may be due to the reversible formation and breaking of the hydrogen bond induced by residual mobility of the molecules. The signal at $\delta_1(^{19}F)$ displays a shorter ^{19}F–^{29}Si distance. All ^{19}F nuclei at $\delta_1(^{19}F)$ are close to a silicon spin. We attribute this population to fluorine atoms in a non-covalent interaction to Q^4 silicon sites, based on electrostatic interactions between the opposite partial charges. This attribution is in line with the predominant Q^4 resonance found in the $^{19}F \rightarrow ^{29}Si$ CP experiments (Figure 5).

In principle, an adsorption in a flat orientation of the molecules on the support is conceivable; nevertheless, such an arrangement is excluded by the absence of proton correlations of the imidazolium and the aromatic moieties with the silica in ^1H–^{29}Si HETCOR spectra at short contact times. At the same time, ^1H–^{19}F (Figure 8) and ^1H–^1H 2D spectra (Figure 9) evidence fluorine or protons at the aromatic ring to be in close proximity to protons of the PEG_2 or the C_{12} chain, respectively. In a completely extended molecular conformation, and a parallel stacking of the IL molecules arranged vertically to the silica surface, these correlations would not be expected. On the other hand, the presence of IL molecules in an antiparallel arrangement, fluorine pointing away from the surface, allows to explain these correlations.

The arrangement of IL molecules might in part be due to their confinement in the mesopores of SBA-15. To assess a possible confinement effect, we have additionally recorded ^{19}F MAS NMR spectra of **2** and **4** deposited on silica with a low pore volume and larger pore size. The ^{19}F chemical shifts and their relative intensities are comparable to those of **SILP-2** and **SILP-4** on SBA-15, indicating a very similar self-assembly of the ILs on a large-pore silica (Figure S35d–f).

Conclusions

Supported Ionic Liquid Phase catalysts have a high potential as stable catalytic materials with improved recyclability. Their potential may be fully exploited if the position of the catalytic center in the IL film can be precisely controlled and finely adjusted. We have presented here a series of new Supported Ionic Liquid Phase materials prepared from four imidazolium-based task-specific ionic liquids $[FPh_nIm^HR]I$ ($n = 1, 2$; $R = PEG_2$, $C_{12}H_{25}$), which are deposited on a mesoporous silica, SBA-15. The structure elucidating power of advanced, multidimensional solid-state NMR spectroscopic techniques allows us to establish a full model of the IL arrangement on the silica. As targeted in the molecular design of these ILs, Coulomb interactions of the charged groups in the molecules and the interactions of fluorine with the silica support induce a self-assembly of the molecules. In consequence, imidazolium cations and iodide anions at the are closely stacked, while either the fluorinated end groups point towards to the silica surface (in a majority of orientations) or point away from the surface in a reversed orientation. MD simulations confirm this model in appealing agreement with the spectroscopic results.

The present work opens the doors for the rational design of a second generation of SILP catalysts, which can self-assemble into an ordered film, aided by specific interactions of a linker moiety with the support surface. In turn, this will allow for positioning a catalytically active metal site at a precise distance to the gas/liquid and the liquid/solid interface. The SILP materials presented here are based on *N*-heterocyclic carbene (NHC) precursors, which can be readily used to prepare catalytic Pt-NHC complexes. The catalytic and structural investigation of those SILP catalysts will be part of a subsequent study.

Supporting Information

The Supporting Information provides details of the IL syntheses, the silica support material, experimental characterization, and the molecular dynamics simulations.

Deposition Number(s) 2297930 (compound **2**) and 2297931 (compound **4**) contain(s) the supplementary crystallographic data for this paper. These data are provided free of charge by

the joint Cambridge Crystallographic Data Centre and Fachinformationszentrum Karlsruhe Access Structures service.

Acknowledgements

The authors thank Rebecca Reber, Dr. Renée Siegel, Antigone Roth, and Dr. Andreas Scheurer for experimental support, and the North Bavarian NMR Centre (NBNC) for measurement time. The authors gratefully acknowledge financial support from the Deutsche Forschungsgemeinschaft (DFG, German Research Foundation) – Project-ID 431791331 – SFB 1452 (CLINT), the Friedrich-Alexander-Universität Erlangen-Nürnberg (FAU) and the Studienstiftung des deutschen Volkes (Ph. D. fellowship to A. B.). Open Access funding enabled and organized by Projekt DEAL.

Conflict of Interests

The authors declare no conflict of interest.

Data Availability Statement

The data that support the findings of this study are openly available in Zenodo at https://zenodo.org/records/10078073, reference number 10078073.

Keywords: ionic liquid · molecular dynamics simulation · solid-state NMR · REDOR · supported ionic liquid phase

[1] M. Logemann, J. M. Marinkovic, M. Schörner, E. José García-Suárez, C. Hecht, R. Franke, M. Wessling, A. Riisager, R. Fehrmann, M. Haumann, *Green Chem.* **2020**, *22*, 5691–5700.
[2] R. Franke, N. Brausch, D. Fridag, A. Christiansen, M. Becker, P. Wasserscheid, M. Haumann, M. Jakuttis, S. Werner, A. Schönweiz, *DE102010041821 A120120405*, **2010**.
[3] M. Abai, M. P. Atkins, A. Hassan, J. D. Holbrey, Y. Kuah, P. Nockemann, A. A. Oliferenko, N. V. Plechkova, S. Rafeen, A. A. Rahman, R. Ramli, S. M. Shariff, K. R. Seddon, G. Srinivasan, Y. Zou, *Dalton Trans.* **2015**, *44*, 8617–8624.
[4] C. Kolbeck, N. Paape, T. Cremer, P. S. Schulz, F. Maier, H. P. Steinrück, P. Wasserscheid, *Chem. Eur. J.* **2010**, *16*, 12083–12087.
[5] S. Shylesh, D. Hanna, S. Werner, A. T. Bell, *ACS Catal.* **2012**, *2*, 487–493.
[6] A. Corma, H. Garcia, *Adv. Synth. Catal.* **2006**, *348*, 1391–1412.
[7] D. Zhao, J. Feng, Q. Huo, N. Melosh, G. H. Fredrickson, B. F. Chmelka, G. D. Stucky, *Science* **1998**, *279*, 548–552.
[8] X. Wang, C. S. Vogel, F. W. Heinemann, P. Wasserscheid, K. Meyer, *Cryst. Growth Des.* **2011**, *11*, 1974–1988.
[9] V. Seidl, A. H. Romero, F. W. Heinemann, A. Scheurer, C. S. Vogel, T. Unruh, P. Wasserscheid, K. Meyer, *Chem. Eur. J.* **2022**, *28*, e202200100.
[10] W. A. Henderson, J. V. G. Young, D. M. Fox, H. C. De Long, P. C. Trulove, *Chem. Commun.* **2006**, 3708–3710.
[11] P. F. Fulvio, S. Pikus, M. Jaroniec, *J. Colloid Interface Sci.* **2005**, *287*, 717–720.
[12] M. Kruk, M. Jaroniec, C. H. Ko, R. Ryoo, *Chem. Mater.* **2000**, *12*, 1961–1968.
[13] M. Thommes, K. Kaneko, A. V. Neimark, J. P. Olivier, F. Rodriguez-Reinoso, J. Rouquerol, K. S. W. Sing, *Pure Appl. Chem.* **2015**, *87*, 1051–1069.
[14] R. E. Youngman, S. Sen, *J. Non-Cryst. Solids* **2004**, *337*, 182–186.
[15] T. M. Duncan, D. C. Douglass, R. Csencsits, K. L. Walker, *J. Appl. Phys.* **1986**, *60*, 130–136.
[16] C. E. Bronnimann, I. S. Chuang, B. L. Hawkins, G. E. Maciel, *J. Am. Chem. Soc.* **1987**, *109*, 1562–1564.
[17] C. C. Liu, G. E. Maciel, *J. Am. Chem. Soc.* **1996**, *118*, 5103–5119.
[18] B. Grünberg, T. Emmler, E. Gedat, I. Shenderovich, G. H. Findenegg, H.-H. Limbach, G. Buntkowsky, *Chem. Eur. J.* **2004**, *10*, 5689–5696.
[19] M. Frosch, C. L. Tavera Mendez, A. B. Koch, M. Schörner, M. Haumann, M. Hartmann, D. Wisser, *J. Phys. Chem. C* **2023**, *127*, 9196–9204.
[20] M. Haumann, A. Schönweiz, H. Breitzke, G. Buntkowsky, S. Werner, N. Szesni, *Chem. Eng. Technol.* **2012**, *35*, 1421–1426.
[21] K. A. Cychosz, M. Thommes, *Engineering* **2018**, *4*, 559–566.
[22] C. Schlumberger, M. Thommes, *Adv. Mater. Interfaces* **2021**, *8*, 2002181.
[23] L. Koenig, in *Spectroscopy of Polymers*, Elsevier, Cleveland, **1999**.
[24] J. W. Wiench, C. Michon, A. Ellern, P. Hazendonk, A. Iuga, R. J. Angelici, M. Pruski, *J. Am. Chem. Soc.* **2009**, *131*, 11801–11810.
[25] K. Mao, T. Kobayashi, J. W. Wiench, H.-T. Chen, C.-H. Tsai, V. S. Y. Lin, M. Pruski, *J. Am. Chem. Soc.* **2010**, *132*, 12452–12457.
[26] T. Gullion, J. Schaefer, *J. Magn. Reson.* **1989**, *81*, 196–200.
[27] T. Gullion, in *Modern Magnetic Resonance*, Springer Netherlands, Dordrecht, **2006**.
[28] R. Jabbour, M. Renom-Carrasco, K. W. Chan, L. Völker, P. Berruyer, Z. Wang, C. M. Widdifield, M. Lelli, D. Gajan, C. Copéret, C. Thieuleux, A. Lesage, *J. Am. Chem. Soc.* **2022**, *144*, 10270–10281.
[29] M. Kashefi, N. Malik, J. O. Struppe, L. K. Thompson, *J. Magn. Reson.* **2019**, *305*, 5–15.
[30] T. Azaïs, S. Von Euw, W. Ajili, S. Auzoux-Bordenave, P. Bertani, D. Gajan, L. Emsley, N. Nassif, A. Lesage, *Solid State Nucl. Magn. Reson.* **2019**, *102*, 2–11.
[31] J. M. Goetz, J. Schaefer, *J. Magn. Reson.* **1997**, *127*, 147–154.
[32] A. Venkatesh, A. Lund, L. Rochlitz, R. Jabbour, C. P. Gordon, G. Menzildjian, J. Viger-Gravel, P. Berruyer, D. Gajan, C. Copéret, A. Lesage, A. J. Rossini, *J. Am. Chem. Soc.* **2020**, *142*, 18936–18945.
[33] C. A. Fyfe, A. R. Lewis, *J. Phys. Chem. B.* **2000**, *104*, 48–55.
[34] M. Macht, B. Becit, D. Zahn, *J. Pharm. Sci.* **2020**, *109*, 2018–2023.

Manuscript received: November 8, 2023
Accepted manuscript online: November 14, 2023
Version of record online: December 4, 2023